Influence of growth temperature on interdiffusion in uncapped SiGe-islands on Si(001) determined by anomalous x-ray diffraction and reciprocal space mapping

T. U. Schülli,[1,2,*] M. Stoffel,[3] A. Hesse,[2] J. Stangl,[2] R. T. Lechner,[2] E. Wintersberger,[2] M. Sztucki,[1] T. H. Metzger,[1] O. G. Schmidt,[3] and G. Bauer[2]
[1]European Synchrotron Radiation Facility, Boîte Postale 220, F-38043 Grenoble Cedex, France
[2]Institute for Semiconductor Physics, Johannes Kepler Universität Linz, A-4040 Linz, Austria
[3]Max-Planck-Institute for Solid State Physics, D-70569 Stuttgart, Germany
(Received 17 March 2004; revised manuscript received 17 September 2004; published 19 January 2005)

The influence of growth temperature in the regime of dome formation in Stranski–Krastanow growth is studied systematically on a series of Ge on Si(001) samples. A combination of complementary x-ray scattering methods is applied, in order to resolve the island size, their strain state, and the composition distribution. The composition is determined using anomalous x-ray diffraction at high momentum transfer in combination with atomic force microscopy and from x-ray reciprocal space mapping. For growth temperatures between 620 and 840 °C, the maximum Ge content of the as-grown islands decreases from about 70 to about 22%. The results are corroborated by a selective etching study of the Ge islands.

DOI: 10.1103/PhysRevB.71.035326 PACS number(s): 68.65.−k, 61.10.Eq, 81.07.−b

I. INTRODUCTION

The self-organized growth of nanometer-sized islands has been intensively studied in the last decade using different material combinations like InAs/GaAs (for a review see, e.g., Refs. 1 and 2) or Ge/Si[3–5] and various deposition methods like chemical vapor deposition or molecular beam epitaxy (MBE). If the island sizes are in the range of the de Broglie wavelength of the charge carriers, quantization effects become important. Therefore, these low-dimensional systems offer a unique opportunity to probe quantum effects. In particular electronic and optical properties are expected to result from the three-dimensional charge carrier confinement in the islands and the zero-dimensional density of states. Among the different material systems, the simple Ge/Si(001) system can be considered as a prototype for understanding the fundamental physical properties related with heteroepitaxial growth. The growth of Ge on Si(001) has therefore been investigated by many different experimental methods.[5,6] The growth starts in a layer-by-layer mode but, due to the 4.2% lattice mismatch between Ge and Si, the strain energy accumulated in the planar layer can be relaxed through nucleation of three-dimensional islands on top of a 3–4 ML thick wetting layer. Depending on the amount of deposited Ge and the substrate temperature, different island morphologies were observed. At moderate temperatures of about 500 °C, {105} facetted and elongated "hut clusters" with edges aligned along ⟨100⟩ directions appear while at slightly higher temperatures of 580 °C, a bimodal mixture consisting of square-shaped pyramids bounded by four {105} facets, and multifacetted "dome"-shaped islands was observed. Finally, at temperatures higher than 600 °C, the majority of the islands are dome-shaped.[7] For any applications of these islands, it is important not only to understand the growth mechanism but also to know the compositional state in the islands. This important question was only recently the subject of several investigations.[8–25] X-ray-based methods were used to determine the composition in SiGe islands,[13,16,21] anomalous diffraction has been applied in Refs. 23 and 24. More recently, the use of a selective etching technique was also used to determine the lateral composition profile in uncapped pyramid islands.[19,22] The same method was also combined with anomalous diffraction to determine the composition in Ge-dome islands grown at 600 °C.[25] However, a detailed analysis of the SiGe intermixing as a function of temperature in Ge-dome islands is still lacking.

In this paper, we use anomalous x-ray diffraction at high momentum transfer to determine the composition of monomodal distributions of Ge domes grown at temperatures between 620 and 840 °C. The results are compared with x-ray reciprocal space maps that yield the strain and the composition in the islands. The composition profiles are also compared with selective etching experiments that allow to identify the Ge rich regions of the islands by comparing atomic force microscopy images before and after etching. The paper is divided in four parts: After the introduction (Sec. I), the experimental methods are presented in Sec. II starting with anomalous diffraction at high momentum transfer (part A), continuing with isostrain scattering (part B) and x-ray reciprocal space mapping (part C). In Sec. III we discuss the experiments and results in detail, a summary is given in Sec. IV.

II. EXPERIMENTAL METHODS

A. Anomalous diffraction at high momentum transfer

The atomic scattering factor for x rays varies considerably for x-ray energies in the vicinity of an atomic energy level. The use of this resonant energy dependence in x-ray scattering experiments is known as anomalous scattering.[26] In a general expression, the atomic scattering factor can be written in the form

$$f(Q,E) = f_0(Q) + f'(E) + if''(E), \quad (1)$$

where $f_0(Q)$ describes the dependence of the scattering factor on the momentum transfer Q. $f_0(Q)$ decreases with higher

 ©2005 The American Physical Society

momentum transfer, as a result of the spatial distribution of the scattering electrons of the atom. The complex resonance correction $f'(E)+if''(E)$ becomes important when the x-ray energy E approaches an absorption edge. For typical x-ray energies used in crystallography, the affected atomic energy levels concern in general the inner shells. For a SiGe alloy, the only accessible absorption edge that can be used for diffraction is the Ge-K edge. Here, the electron shells responsible for the resonant correction terms $f'(E)$ and $f''(E)$ have an electron density distribution with a maximum in the vicinity of the nucleus. Their localization in space justifies the disregard of their dependence on the momentum transfer Q. The resonant corrections $f'(E)$ and $f''(E)$ being small compared to $f_0(Q)$ in the case of forward scattering (i.e., at $Q=0$) therefore gain in importance if the scattering experiments are carried out at high Q values. To determine the composition in a SiGe alloy, a change in the scattered intensity in the vicinity of the Ge-K edge can be attributed to a certain Ge concentration, if the dependence of Eq. (1) on Q and E is quantitatively known. The determination of the correction terms is generally done by an energy-dependent measurement of absorption, being a measure for $f''(E)$. The absorption is measured with high energy resolution in the vicinity of the absorption edge, and supplemented by tabulated values (we used those of Ref. 27) for the remaining part of the energy spectrum. The calculation of the dispersive part $f'(E)$ from the measured $f''(E)$ is done via a Kramers–Kronig transfomation. The values for the momentum dependent part $f_0(Q)$ of Eq. (1) are calculated using the parameterized model according to Ref. 28.

For kinematic scattering, the diffracted intensity of a Bragg peak is proportional to $|f(Q,E)|^2$. When $f(Q,E)$ changes for two energies E_1 and E_2, one can therefore determine the ratio between the average moduli. Considering an alloy of $Si_{1-c}Ge_c$, the diffracted intensity at all fundamental Bragg reflections of the diamond structure is proportional to the square of the average alloy scattering factor $\bar{f}$. The intensity ratio for the two probed energies E_1 and E_2 then reads

$$\frac{I_{E_1}}{I_{E_2}} = \left|\frac{\bar{f}_{E_1}}{\bar{f}_{E_2}}\right|^2 = \left|\frac{c[f_{0_{\mathrm{Ge}}}(Q)+f'_{\mathrm{Ge}_{E_1}}+if''_{\mathrm{Ge}_{E_1}}]+(1-c)[f_{0_{\mathrm{Si}}}(Q)+f'_{\mathrm{Si}}+if''_{\mathrm{Si}}]}{c[f_{0_{\mathrm{Ge}}}(Q)+f'_{\mathrm{Ge}_{E_2}}+if''_{\mathrm{Ge}_{E_2}}]+(1-c)[f_{0_{\mathrm{Si}}}(Q)+f'_{\mathrm{Si}}+if''_{\mathrm{Si}}]}\right|^2. \quad (2)$$

To exploit the momentum dependence of $f_{0_{\mathrm{Ge}}}$ the experiments should be performed at a high indexed Bragg reflection. Furthermore, the two energies E_1 and E_2 were chosen below the Ge-K-edge energy to avoid a rise of the momentum-independent scattering contribution of the imaginary part if''_{Ge} at values too close or at the K edge. In addition this prevents an increased background due to Ge fluorescence. Figure 1(a) shows line plots of the resonant corrections for Ge in the vicinity of $E_{K_{\mathrm{Ge}}}=11\,103$ eV. Two vertical lines mark the energies $E_1=11\,043$ eV and $E_2=11\,102$ eV. In Fig. 1(b) the momentum dependence of the real parts of f_{Ge} and f_{Si} are plotted for these energies. The relative change of f_{Ge} increases dramatically for higher Q values. This leads to an important enhancement of the anomalous effect and therefore to an increase in the intensity ratio in Eq. (2). Except for the Ge content c all quantities in Eq. (2) can be calculated or measured independent of the diffraction experiment. As f'_{Si} and f''_{Si} are constant in the considered energy interval, the measured intensity ratio can be unambiguously linked to the Ge content. An important point for the concentration determination by anomalous scattering is the quantitative reliability of the determination of $|[f_{\mathrm{Ge}}(Q,E)]|$ for the concerned energy ranges *and* momentum transfers. Sources of errors lie in the absorption measurement of f''_{Ge}, the reliability of the tabulated values, and the integration range chosen for the evaluation f'_{Ge}. Furthermore it seems to be adequate to have a measure in order to confirm the validity of the momentum dependency of $f_0(Q)$ calculated according to Ref. 28. As the modulus of the atomic scattering factor will be the quantity probed by the measurement of scattered x-ray intensities, it is most suitable to check the validity of $|f_{\mathrm{Ge}}(Q)|$ as derived from Eq. (1). This is done by a comparison of the scattered intensities from pure Ge for a range of energies and different Bragg reflections (different momentum transfers) with the theoretically derived values. To assure the propor-

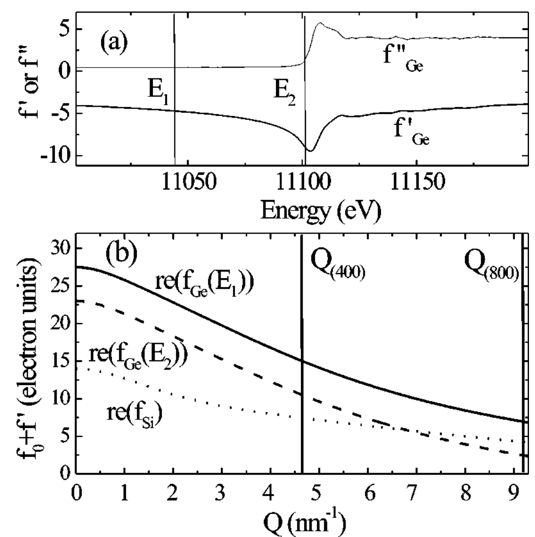

FIG. 1. (a) Resonant correction terms f'_{Ge} and f''_{Ge} in the vicinity of the K-absorption edge. (b) Real part of the complex atomic scattering factors for Ge (full and dashed line) at the energies marked in (a), and real part of f_{Si}.

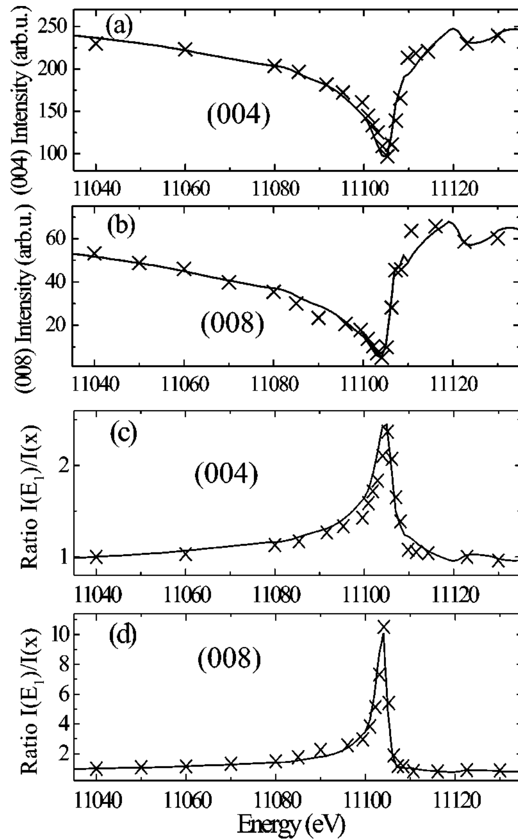

FIG. 2. (a) and (b) Measured (crosses) and calculated (full line) integrated intensities of the (004) (a) and (008) (b) Bragg reflections of a thin Ge film as a function of energy across the Ge-K edge. (c) and (d). Measured (crosses) and (calculated) intensity ratio between the scattered x-ray intensity at $E_1 = 11\,043$ eV and all other measured energies in the vicinity of the Ge-K edge at the (004) reflection in (c) and the (008) reflection in (d).

tionality between the modulus of the atomic scattering factor with the integrated intensity of a Bragg reflection, the pure Ge sample used for such a calibration measurement has to be a kinematic scatterer, i.e., multiple scattering events have to be negligible. We used here a 30 nm thick highly mosaic Ge film grown at 150 °C on Si(001) to fulfill these requirements. Additionally, absorption corrections can be neglected for a 30 nm large scattering object, even for x-ray energies above the K-absorption edge. This simplification also holds for all investigated samples in this work. Figures 2(a) and 2(b) show such a calibration measurement for the diffracted intensities (crosses) across the (004) reflection (a) and the (008) reflection (b) as a function of energy. Both measurements are compared with the calculated energy dependence of the diffracted intensity (full lines). In Figs. 2(c) and 2(d), the intensity ratio between the measured intensity at $E_1 = 11\,043$ eV and all other measured points in the curve is plotted (crosses) for both reflections. The full lines represent the calculated intensity ratios according to Eq. (2) for $c=1$ with the theoretical input values for $f_{0_{Ge}}(Q)$, $f'_{Ge}(E)$, and $f''_{Ge}(E)$ determined as described earlier. Figure 2 shows a good agreement between the calculated and measured intensity ratios for pure Ge. It is important to note that the intensity minimum for the Ge (004) reflection lies at 11 103 eV, whereas for the (008) reflection it is found 1 eV below the K edge at 11 102 eV. This is explained by the strong influence of the momentum transfer on the real part of the atomic scattering factor. With decreasing $f_{0_{Ge}}(Q)$ for high Q values, the real part $f_{0_{Ge}}(Q)+f'_{Ge}$ decreases. As the imaginary part contains no Q dependence, its steep rise at the K edge becomes a more important contribution to the absolute value of $|f_{Ge}|$ for high momentum transfer. It, hence, causes a rise in intensity at the K edge for the (008) reflection and thus shifts the minimum in $I \propto |f_{Ge}(E)|$ to lower energies than the K edge. The change of the maximum value for the intensity ratio between the (004) and the (008) reflection clearly underlines the benefit gained by performing anomalous scattering at high momentum transfer. A study of this influence on a number of Bragg reflections in the SiGe system has been published earlier.[24]

B. Shape analysis in isostrain scattering

In order to investigate the correlation of strain and lateral size in quantum dots, Kegel *et al.* have published a method called isostrain scattering.[29] It is based on the fact that two regions with different lattice parameter scatter at different positions in the radial direction ($\|\mathbf{Q}$) in reciprocal space. A scan perpendicular to this direction, a so-called angular scan, therefore has a line shape that is entirely defined by size and shape in real space of the region with the corresponding lattice parameter. Recently, this method has been combined with anomalous diffraction in order to correlate strain, composition, and size of SiGe islands.[24] In this report, we use the (800) in-plane reflections of our samples to determine the composition as a function of lattice parameter by anomalous diffraction from the radial scans. In a second step, angular scans are recorded perpendicular to the radial direction. For any of these, the lateral size of a region with distinct lattice parameter is determined. As uncapped epitaxial islands relax monotonically from bottom to the top, the lateral size of the SiGe domes decreases with increasing relaxation. This finally limits the resolution of the isostrain scattering method. As the form factor for a region with common lattice parameter also expands in radial direction, the overlap of these regions in reciprocal space becomes more important for broad shape functions, thus for regions that are small in real space. As the strain broadening of Bragg reflections increases with momentum transfer (with the order of the reflection) but the size broadening stays constant, the size resolution also depends on the chosen Bragg reflection. As shown in Ref. 29 a lattice parameter discrimination $\Delta a/a$ is possible when the condition

$$\frac{2\pi}{R} < \frac{\Delta a}{a} Q \tag{3}$$

is fulfilled, where R is the lateral size of an isostrain volume. As an example, for two regions differing by 0.3% in lattice parameter, and at the momentum transfer of the Si(400) reflection, the size limit lies at about $R=45$ nm.

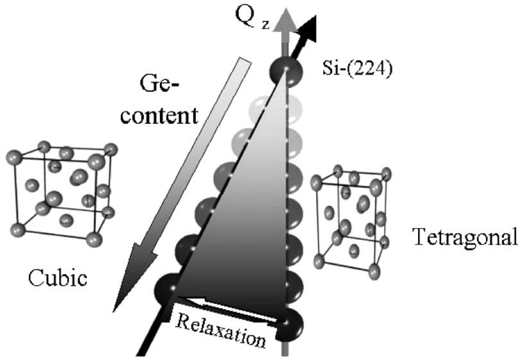

FIG. 3. Relaxation triangle in reciprocal space for a SiGe alloy epitaxially grown on Si(001). As an example, the vicinity of the asymmetric Si(224) Bragg point is sketched.

C. X-ray reciprocal space mapping

The second x-ray method giving access to strain and interdiffusion of self-organized islands is x-ray reciprocal space mapping. The method is based on the knowledge of the elastic properties as well as the lattice parameters of Si, Ge, and SiGe alloys. In the case of [001] as the growth direction, one considers the Poisson-ratio ν_{100} to calculate the response of a crystal that is deformed from its native lattice constant a to a value $a_{\parallel}$ in the growth plane. The corresponding change of the lattice parameter in growth direction $a_{\perp}$ is then calculated by

$$a_{\perp} = a\left(1 + \frac{a - a_{\parallel}}{a_{\parallel}} \frac{1 + \nu_{100}}{1 - \nu_{100}}\right). \tag{4}$$

We can therefore measure $a_{\parallel}$ and $a_{\perp}$ which is the response to $a_{\parallel}$ and use the knowledge about ν_{100} to derive the equilibrium lattice parameter a. Together with the lattice parameter interpolation in SiGe alloys,[30,31] this leads to a determination of the composition of the SiGe alloy. In the Stranski–Krastanow growth mode of islands, the material is partially elastically relaxed, with the degree of relaxation increasing with the height inside the islands. In order to obtain information about strain and composition, the scattered intensity in the vicinity of asymmetric Bragg reflections is measured.[16,21]. In Fig. 3, the situation is sketched for SiGe islands on Si(001) in the vicinity of the (224) Bragg point of Si. As Ge has a larger lattice constant than Si (a_{Ge} $=564.6$ pm, $a_{Si}=543.1$ pm), one expects to observe the scattered intensity from crystalline Ge or SiGe alloys to be closer to the reciprocal origin than the Si-reciprocal lattice point. In the case of perfect pseudomorphic growth ($a_{\parallel}=a_{Si}$), the scattered intensity from the distorted crystal will be found at the same Q_x value as the Si-Bragg point at a distance in Q_z which is purely defined by the composition. For complete relaxation, the crystal will be cubic and hence its scattered intensity will be found on the "cubic path," i.e., the connection between the origin of reciprocal space and the Si-reciprocal lattice point. A change in composition by enrichment in Si of the SiGe alloy will in both cases shift the intensity towards the Si-Bragg point. Thus a variation of composition will lead to an intensity distribution in a radial direction from the Si-reciprocal lattice point for both, the relaxed and the pseudomorphic case. A change in relaxation between these extreme states will lead to an intensity distribution along an isocomposition line as indicated in Fig. 3. In order to analyze the reciprocal space maps, we assume SiGe islands with the shape of a rotational paraboloid with base width and height according to the atomic force microscopy (AFM) data. The Ge composition inside the island is chosen to vary in a square-root manner from a value c_1 at the island bottom (the wetting layer is assumed to have the same chemical composition) to a value c_2 at the island top.

TABLE I. Growth parameters of the investigated samples. The amount of Ge deposited by MBE is given in atomic monolayers. The base width and the height of the islands is deduced from AFM scans. The dome width is slightly overestimated due to the AFM tip convolution effect.

Sample	A	B	C	D
T (°C)	620	700	750	840
d_{Ge} (ML)	6.7	11	11	6
Dome-width (AFM) (nm)	87	143	170	338
Dome-height as grown (AFM) (nm)	19	36	34	37
Dome-height after etching (AFM) (nm)	13	36	34	37

From this composition profile, the strain field inside the island is calculated using finite elements, taking the anisotropic elastic behavior of SiGe into account. For the elastic constants, we use a linear interpolation between the values of Si and Ge.

From the displacement field integrated from the strain, the scattered intensity distribution is calculated by means of the distorted wave Born approximation, as described in detail in Ref. 16. The values c_1 and c_2 are varied iteratively, until a good correspondence between simulation and experiment is achieved.

III. EXPERIMENTS

A. Sample growth

The investigated samples were grown by solid source molecular beam epitaxy (base pressure 1×10^{-10} mbar). Si was evaporated with an electron beam evaporator while Ge was evaporated from an effusion cell. The typical deposition rates are 0.1 and 0.005 nm/s for Si and Ge, respectively. After oxide desorption and growth of a 100 nm thick Si-buffer layer, 6–11 ML Ge were deposited at various temperatures ranging from 620 to 840 °C. The substrate temperature is calibrated by measuring the voltage over a thermocouple mounted on a n-Si(001) wafer under identical growth conditions which results in an accuracy of 20 °C. Table I presents the sample structure as well as the width and height of the islands deduced from AFM scans.

At the growth temperatures used, dome shaped islands are commonly observed. The Ge deposition was chosen so that a monomodal distribution of dome islands was obtained. Figure 4(a) shows a 10×10 μm AFM image from the sample A. We can easily see that a very homogeneous distribution of dome islands is obtained. A statistical analysis [Figs. 4(b)

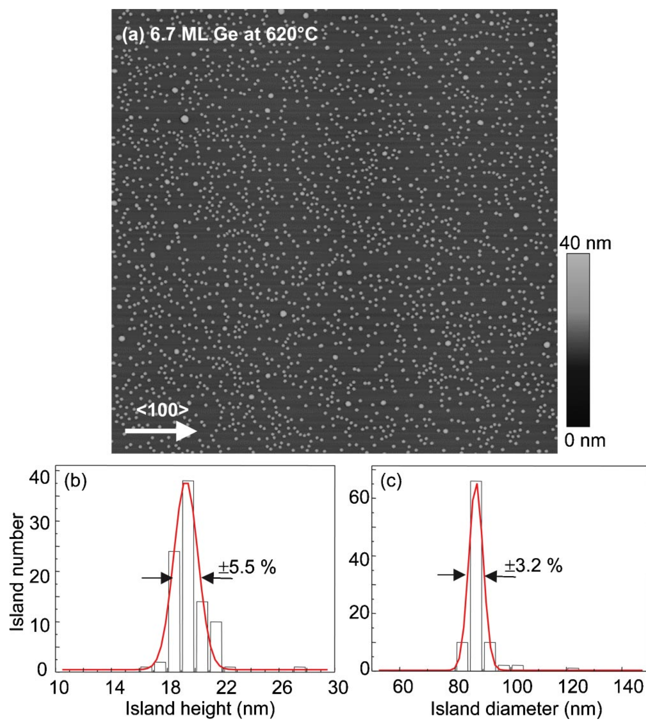

FIG. 4. (a) AFM image (10×10 μm) obtained after deposition of 6.7 ML Ge at 620 °C (b) island height distribution (c) island diameter distribution.

and 4(c)] shows that the island height distribution can be fitted with a Gaussian curve having a full width at half maximum (FWHM) of $\pm5.5\%$ while the island diameter distribution has a FWHM of only 3.2%. At higher growth temperatures, the dome size increases but the aspect ratio remains almost constant in the temperature range from 620 to 750 °C, as can be obtained from AFM images shown in Fig. 5. For growth at 840 °C, the aspect ratio is drastically different and one observes an intermediate shape between pyramids and domes. The AFM images of all investigated samples are shown in Fig. 5. Transmission electron micrographs of cross

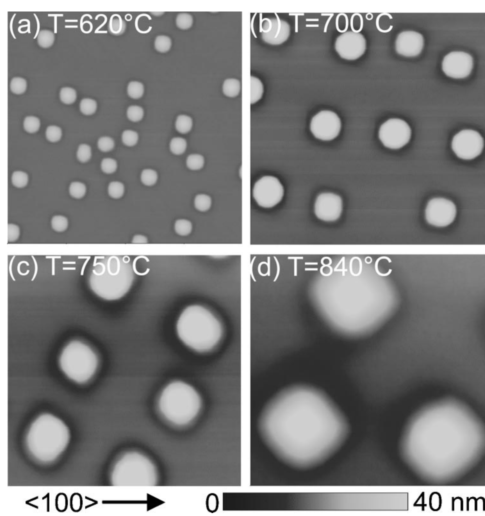

FIG. 5. AFM images (1×1 μm^2) of the investigated samples. The growth temperature increases from (a) through (d) as indicated.

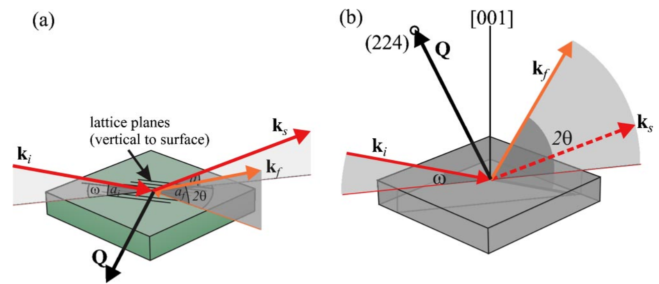

FIG. 6. Scattering geometries as used in the x-ray experiments. (a) Grazing incidence (k_i) and -exit (k_f) of the x-ray beam allows to excite diffraction from lattice planes perpendicular to the surface. The momentum transfer **Q** thus lies in the sample surface. (b) The coplanar diffraction geometry for a [001] surface. Incident (k_i) and scattered (k_f) x-ray beams lie in the same plane then the surface normal.

sections of the samples show that the islands are not dislocated and contain no stacking faults. More informations about growth can be found in Ref. 10. In order to quantify the composition in the islands, we first investigate the islands using anomalous diffraction.

B. Anomalous diffraction

The anomalous diffraction measurements were performed at the beamline ID01 at the European Synchrotron Radiation Facility in Grenoble, France. Radial scans across the (800) surface reflection were recorded using the grazing incidence diffraction setup as sketched in Fig. 6(a). Figure 7(a) shows

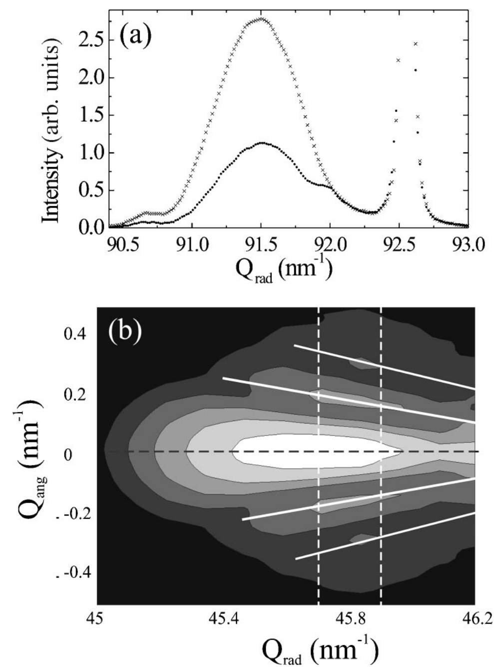

FIG. 7. (a) Radial scans for two energies $E_1=11\,043$ eV (crosses) and $E_2=11\,102$ eV (dots) across the (800) in-plane reflection of sample B. (b) In-plane reciprocal space map of the (400) reflection composed of a series of angular scans, perpendicular to the scan direction in (a).

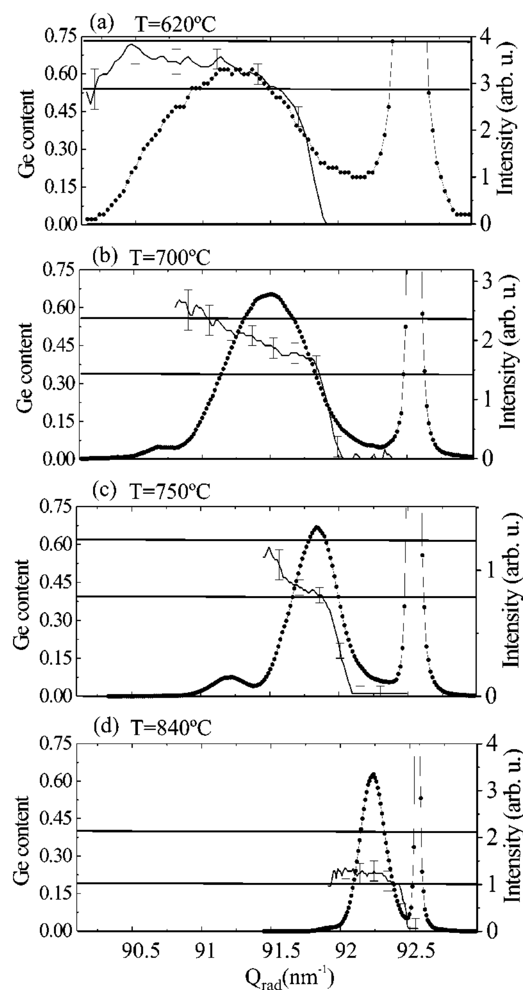

FIG. 8. Ge content (line plots) extracted from radial scans across (800) in-plane reflection for two different energies. (a)–(d) represent increasing growth temperature of the samples from Table I. On the same Q scale, the diffracted intensity at the (800) reflection as recorded at 11 043 eV is plotted (connected dots). Horizontal lines indicate the bandwidth of the Ge concentration inside the islands as determined by x-ray-reciprocal space mapping.

two radial scans for the energies $E_1=11\,043$ eV (crosses) and $E_2=11\,102$ eV (dots) for the sample B, grown at 700 °C. The silicon (800) Bragg peak situated at 92.55 nm^{-1} is not shown to the full intensity. The intensity distribution between 90.5 and 92.0 nm^{-1} is attributed to the strained SiGe island. For momentum transfers higher than 92.0 nm^{-1} one observes no change in the scattered intensity between the two spectra. Therefore this region corresponds to pure Si and, hence, represents the scattering from strained Si below the SiGe island. As 92.0 nm^{-1} correspond to a lattice parameter of 546 pm, the maximum strain in the Si at the surface amounts to 0.6% for this sample. With the knowledge about the atomic scattering factors of Si and Ge and the use of Eq. (2), one can now extract the Ge content in reciprocal space from the scans in Fig. 7(a). The results of this procedure are shown for all four samples in Figs. 8(a)–8(d) as a full line. For clarity, the scattered intensity distribution across the (800) reflection is plotted (connected dots). Both curves allow a better interpretation of the Ge distribution inside the islands. The evolution of the Ge content as plotted in Figs. 8(a)–8(c), follows a similar behavior for growth temperatures from 620 to 750 °C. One observes an extended region between the reciprocal positions of the Si substrate and the SiGe island where only Si contributes to the diffracted signal. Scattering in this region is thus caused by strained Si in the substrate area below the SiGe island. This region shrinks with higher temperatures, indicating that the substrate is less tensile strained for higher growth temperatures. The maximum strain in the Si can be determined from these graphs to be 0.75% (A, 620 °C), 0.6% (B, 700 °C), 0.5% (C, 750 °C), and $<0.1\%$ (D, 840 °C). It is visible from Figs. 8(a)–8(c), that in the temperature regime below 800 °C, the Ge concentration evolves abruptly at a certain lattice parameter position at the substrate/island interface. Beyond this point, the composition gradient inside the island shows a rather flat evolution, however, with a slightly higher gradient for higher growth temperatures, indicating increasing intermixing. The data demonstrate that despite the intermixing of the islands, a relatively sharp interface between the Si substrate and the SiGe island remains. If SiGe intermixing would take place through the bottom interface, a smooth evolution of the composition could be expected. Hence, our results indirectly support growth models, which suggest that Si diffusion is strain-driven:[8,9,19,20] Since the regions around the circumference of the islands are the ones with the highest strain values, Si diffuses mainly from there into the islands, leading to the formation of trenches around the island bases. The sample grown at 840 °C shows a qualitatively different behavior, which is also corroborated by the other methods as explained later.

For each sample, a series of angular scans at different radial positions was recorded. They are plotted as an intensity map in Fig. 7(b) for the (400) reflection. The black dashed line at $Q_{\text{ang}}=0$ represents the radial scan direction, for which the scan in (a) is recorded. It is the direction in which the lattice parameter distribution is measured. Two white dashed lines indicate angular scans. As a guide to the eye, full white lines indicate the maxima positions of the finite size oscillations. These fringes are present in the angular scans at a fixed position Q_{rad} and are caused by the well-defined finite size of the diffracting region with a common lattice parameter. Their enlargement for smaller Q_{rad} (i.e., for larger lattice parameters) is caused by the fact that the more relaxed parts of the domes are found at the apex, where the lateral size of the island is smaller. They finally vanish in the low-Q_{rad} regime, as the diffracting regions are too small to fulfill the resolution criterion from Eq. (3). A comparison of the widths obtained from the angular scans with AFM line scans is used to link the lattice parameter with a certain height above the substrate surface. As the dependence between lattice parameter and Ge concentration has been determined before, this allows to establish the Ge content as a function of the height inside the island. The result is shown for the growth temperatures 620–750 °C in Fig. 9.

C. Reciprocal space maps

For all investigated samples, coplanar reciprocal space maps were recorded in the vicinity of the (224) Bragg reflec-

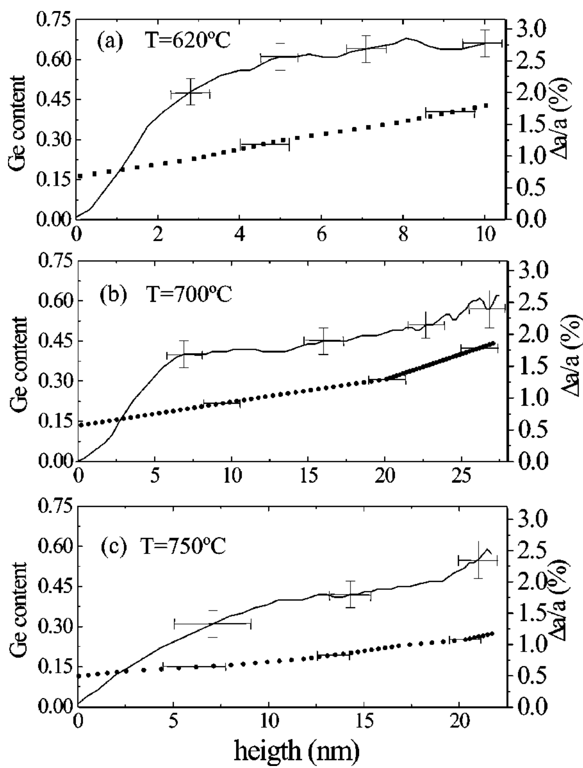

FIG. 9. Ge-content (line plots) as a function of height for the growth temperature regime 620–750 °C. The lattice parameter relaxation $\Delta a/a$ with respect to the lattice parameter of Si $a_{Si} = 543.1$ pm is added as full symbols.

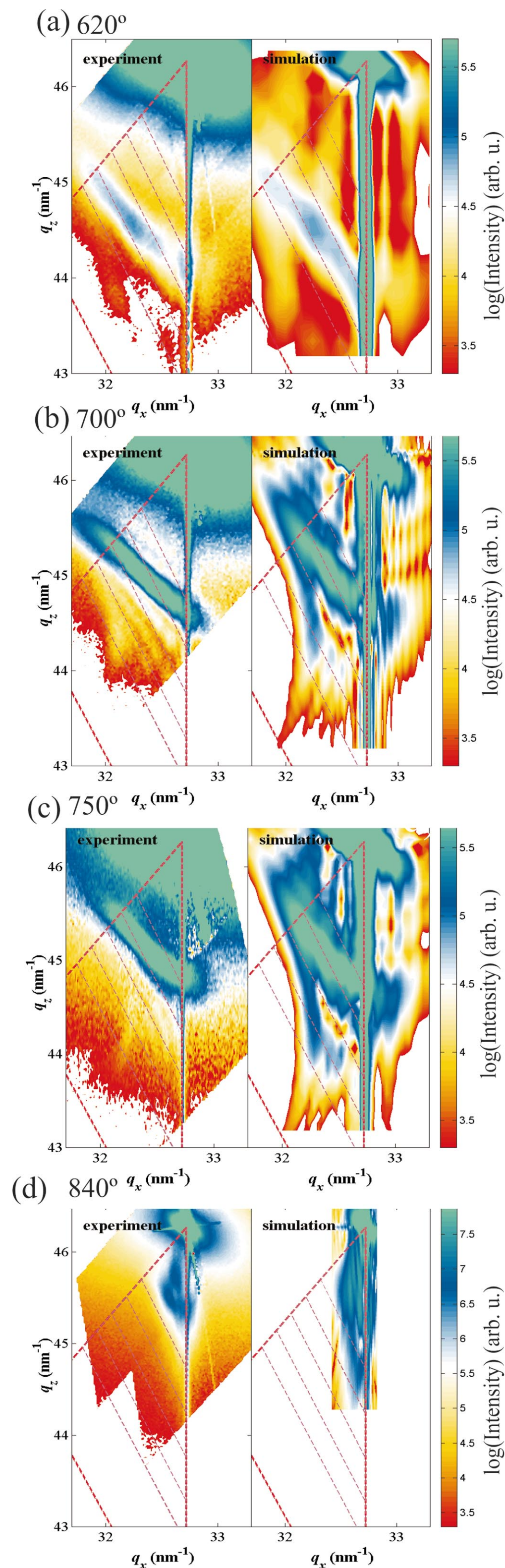

FIG. 10. (Color) Reciprocal space maps of the (224) reflection for four samples (left), together with their finite element simulations (right). The isocomposition lines correspond to the Ge concentrations 30, 40, 50, 60, and 70%.

tion in coplanar scattering geometry as shown in Fig. 6(b). The measuared two-dimensional datasets are plotted in Figs. 10(a)–10(d) (left panels). Beside the substrate peak and the truncation rod, the diffuse intensity distribution originating from the SiGe islands is visible below the reciprocal lattice point of Si. The scattered intensity distribution originating from the SiGe islands has an elongated shape that is almost parallel to the isocomposition lines. This intensity streak approaches the Si-Bragg point for higher temperatures, without changing its inclination with respect to the isocomposition lines. It, hence, clearly pronounces a rather small gradient of the Ge content inside the island. The absolute gradient contributes to a variation of 20% of the Ge concentration throughout the island. The growth characteristics seem not to change between 620 and 750 °C. The average Ge content decreases for higher temperatures, but all samples show small composition gradients inside the islands. The strain in the islands ranges from almost pseudomorphic at the base to almost relaxed at the apex. For temperatures higher than 800 °C the AFM images show an intermediate shape between domes and pyramids, and the growth behavior is different from that observed for 620–750 °C. The intensity distribution in Fig. 10(d) no longer has the elongated shape along the isocomposition lines. We believe that this is due to the reduced strain, which results from enhanced SiGe intermixing: For low average mismatch values, pyramidal-shaped islands are thermodynamically more stable than dome-shaped ones.[32–34] The results of the calculated intensity distribution based on finite-element simulations are presented in the right panels of Figs. 10(a)–10(d). The position and shape of the SiGe-island peaks are reproduced very well in the

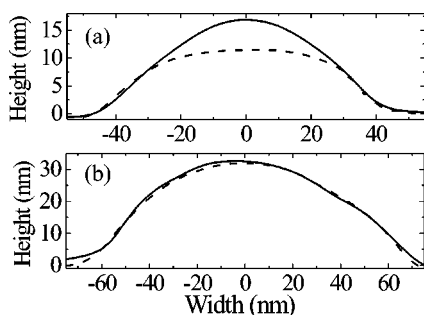

FIG. 11. (a)–(b) AFM cross-sectional profiles of Ge-dome islands grown at 620 °C (a) and at 700 °C (b) before (full line) and after wet chemical etching (dashed line) in a hydrogen peroxide solution.

simulations. In the measurements pronounced diffused scattering around the Si-substrate peaks stems from point defects and thermal diffuse scattering. These phenomena are not taken into account in the simulations. The obtained Ge concentration values at the bottom and the top of the islands are added as horizontal bars to plots of the composition determined by anomalous diffraction in Figs. 8(a)–8(d). Obviously, both methods confirm each other well for the samples grown between 620 and 750 °C. For growth at 840 °C, the agreement between reciprocal space mapping and the anomalous diffraction technique is somewhat worse. As mentioned before, the shape of the islands grown at 840 °C differs from the one grown at lower temperatures. The assumption of a paraboloidal shape overestimates the elastic relaxation and hence might lead to the discrepancy in the concentration determination of the two x-ray diffraction methods.

D. Selective etching

In order to determine the Ge-rich portion of the pyramids, the samples were dipped for two minutes in a 31% H_2O_2 solution, which etches pure Ge and SiGe alloys with Ge contents higher than 65% but neither Si-rich SiGe alloys nor pure Si.[10,22,35] The comparison of AFM scans taken before and after etching allows us to identify the Ge-rich regions of the dome islands. A qualitative comparison can therefore be done with the results obtained by x-ray diffraction. Figure 11 represents AFM cross-sectional profiles of Ge-dome islands grown at 620 °C [sample A, panel (a)] and at 700 °C [sample B, panel (b)] before and after etching in a hydrogen peroxide solution. The shown profiles are averaged over a large ensemble of dome islands. When the island growth temperature increases to 700 °C or more, only small changes occur after etching as can be seen in Fig. 11(b). As we could expect, a higher growth temperature leads to an enhanced intermixing with Si. From the etching experiments, we can conclude that the average Si content in the island is higher than 35%. This is confirmed by anomalous diffraction as well as in the reciprocal space mapping results. In neither of the cases a Ge concentration of more than 65% is derived for sample B. Sample A, however, exceeds 65% Ge at the island apex as determined by both x-ray methods.

IV. SUMMARY

We have investigated systematically the intermixing in SiGe islands on Si(001) as a function of substrate temperature during growth in the range from 620 to 840 °C. The island size increases with growth temperature, whereas the Ge content decreases. The evolution of the Ge concentration inside the islands has been determined by anomalous x-ray scattering and from x-ray reciprocal space maps. The results of both methods agree very well, and are further corroborated by selective etching of Ge-rich parts of the islands. For growth temperatures between 620 and 750 °C, the island formation leaves a well-defined interface between the SiGe island and pure Si. The lattice parameter relaxes from almost pseudomorphic at the island base to completely relaxed at the island top. Despite the pronounced SiGe intermixing, no bluring of the interface between the island and the Si substrate occurs. This supports growth models suggesting Si interdiffusion from the rim of the island base rather than through the whole bottom interface. At 840 °C a substantial change of island shape from domes to pyramids is observed, consistent with the thermodynamic equilibrium shape for increased SiGe interdiffusion.

ACKNOWLEDGMENTS

The technical support from the beamline staff at ID01 at the ESRF is greatly acknowledged. This work was supported by the FWF (No. 14684), Vienna and the EC (No. HPRN-CT-1999-0123 "SiGeNet"). T.U.S. would like to thank the ESRF for a grant.

---

*Present address: CEA Grenoble, DRFMC/SP2M, 17 rue des martyrs, F-38054 Grenoble, France. Electronic address: schulli@esrf.fr

[1] D. Bimberg, M. Grundmann, N. N. Ledentsov, *Quantum Dot Heterostructures* (Wiley, Chichester, 1999).
[2] V. Shchukin, N. N. Ledentsov, and D. Bimberg, *Epitaxy of Nanostructures* (Springer, Berlin, 2003).
[3] K. Brunner, Rep. Prog. Phys. **65**, 27 (2002).
[4] Y. W. Mo, D. E. Savage, B. S. Swartzentruber, and M. G. Lagally, Phys. Rev. Lett. **65**, 1020 (1990).
[5] B. Voigtlaender, Surf. Sci. Rep. **43**, 127 (2001).
[6] F. M. Ross, R. M. Tromp, and M. C. Reuter, Science **286**, 1931 (1999).
[7] R. E. Rudd, G. A. D. Briggs, A. P. Sutton, G. Medeiros-Ribeiro, and R. S. Williams, Phys. Rev. Lett. **90**, 146101 (2003).
[8] X. Z. Liao, J. Zou, D. J. H. Cockayne, J. Qin, Z. M. Jiang, X. Wang, and R. Leon, Phys. Rev. B **60**, 15 605 (1999).
[9] S. A. Chaparro, J. Drucker, Y. Zhang, D. Chandrasekhar, M. R. McCartney, and D. J. Smith, Phys. Rev. Lett. **83**, 1199 (1999).
[10] O. G. Schmidt and K. Eberl, Phys. Rev. B **61**, 13 721 (2000).

[11] G. Capellini, M. De Seta, and F. Evangelisti, Appl. Phys. Lett. **78**, 303 (2001).
[12] A. V. Kolobov, H. Oyanagi, K. Brunner, P. Schittenhelm, G. Abstreiter, and K. Tanaka, Appl. Phys. Lett. **78**, 451 (2001).
[13] J. Stangl, A. Daniel, V. Holy, T. Roch, G. Bauer, I. Kegel, T. H. Metzger, T. Wiebach, O. G. Schmidt, and K. Eberl, Appl. Phys. Lett. **79**, 1474 (2001).
[14] U. Denker, O. G. Schmidt, N. Y. Jin-Phillip, and K. Eberl, Appl. Phys. Lett. **78**, 3723 (2001).
[15] O. G. Schmidt, U. Denker, S. Christiansen, and F. Ernst, Appl. Phys. Lett. **81**, 2614 (2002).
[16] A. Hesse, J. Stangl, V. Holý, T. Roch, G. Bauer, O. G. Schmidt, U. Denker, and B. Struth, Phys. Rev. B **66**, 085321 (2002).
[17] P. Sonnet and P. C. Kelires, Phys. Rev. B **66**, 205307 (2002).
[18] Y. Zhang and J. Drucker, J. Appl. Phys. **93**, 9583 (2003).
[19] U. Denker, M. Stoffel, and O. G. Schmidt, Phys. Rev. Lett. **90**, 196102 (2003).
[20] Ph. Sonnet and P. C. Kelires, Appl. Phys. Lett. **85**, 203 (2004).
[21] Th. Wiebach, M. Schmidbauer, M. Hanke, H. Raidt, R. Köhler, and H. Wawra, Phys. Rev. B **61**, 5571 (2000).
[22] U. Denker, M. W. Dashiell, N. Y. Jin-Phillipp, and O. G. Schmidt, Mater. Sci. Eng., B **89**, 166 (2002).
[23] R. Magalhães-Paniago, G. Medeiros-Ribeiro, A. Malachias, S. Kycia, T. I. Kamins, and R. S. Williams, Phys. Rev. B **66**, 245312 (2002).
[24] T. U. Schülli, J. Stangl, Z. Zhong, R. T. Lechner, M. Sztucki, T. H. Metzger, and G. Bauer, Phys. Rev. Lett. **90**, 066105 (2003).
[25] A. Malachias, S. Kycia, G. Medeiros-Ribeiro, R. Magalhaes-Paniago, T. I. Kamins, and R. S. Williams, Phys. Rev. Lett. **91**, 176101 (2003).
[26] G. Materlik, C. J. Sparks, and K. Fisher, *Resonant Anomalous X-Ray Scattering: Theory and Applications* (North-Holland, Amsterdam, 1994).
[27] B. L. Henke, E. M. Gullikson, and J. C. Davis, At. Data Nucl. Data Tables **54**, 181 (1993).
[28] J. Baró, M. Roteta, J. M. Fernández-Varea, and F. Salvat, Radiat. Phys. Chem. **44**, 531 (1994).
[29] I. Kegel, T. H. Metzger, A. Lorke, J. Peisl, J. Stangl, G. Bauer, J. M. García, and P. M. Petroff, Phys. Rev. Lett. **85**, 1694 (2000).
[30] J. P. Dismukes, L. Ekstrom, and R. J. Paff, J. Phys. Chem. **68**, 3021 (1964).
[31] D. De Salvador, M. Tormen, M. Berti, A. V. Drigo, F. Romanato, F. Boscherini, J. Stangl, S. Zerlauth, G. Bauer, L. Colombo, and S. Mobilio, Phys. Rev. B **63**, 045314 (2001).
[32] A. Rastelli, M. Kummer, and H. von Känel, Physica E (Amsterdam) **13**, 1008 (2002).
[33] P. Sutter, and M. G. Lagally, Phys. Rev. Lett. **81**, 3471 (1998).
[34] T. I. Kamins, E. Medeiros-Ribeiro, E. A. A. Ohlberg, and R. S. Williams, Appl. Phys. A: Mater. Sci. Process. **67**, 727 (1998).
[35] W. Primak, R. Kampwirth, and Y. Dayal, J. Electrochem. Soc. **114**, 88 (1967).